Chemistry – A European Journal

ChemEurJ Chemistry Europe European Chemical Societies Publishing

RESEARCH ARTICLE OPEN ACCESS

Modulating the Optoelectronic Properties of Tripodal Fluorophores Through Fluorine-Substituted Peripheral Phenyls

Milan Klikar[1] | Eva Prokopová[1] | Lefteris Laleas[2] | Giorgos Soultse[2] | Alexandros Katsidas[2] | Zdeňka Růžičková[3] | Zuzana Burešová[1] | Oldřich Pytela[1] | Filip Bureš[1] | Mihalis Fakis[2]

[1]Institute of Organic Chemistry and Technology, Faculty of Chemical Technology, University of Pardubice, Pardubice, Czechia | [2]Department of Physics, University of Patras, Patras, Greece | [3]Department of General an Inorganic Chemistry, Faculty of Chemical Technology, University of Pardubice, Pardubice, Czechia

Correspondence: Milan Klikar (milan.klikar@upce.cz)

Received: 18 November 2025 | **Revised:** 9 December 2025 | **Accepted:** 18 December 2025

Keywords: C_3-symmetric fluorophores | DFT calculations | fluorination effect | intramolecular charge transfer (ICT) | two-photon absorption (2PA)

ABSTRACT

Fourteen novel tripodal fluorophores based on a central triphenylamine donor, electron-rich, and polarizable divinylthiophene linker, and eight different fluorine-based substituents have been designed and prepared via a straightforward four-step sequence. Altering the peripheral F-substitution has been demonstrated to largely affect their fundamental properties such as thermal robustness (210–420 °C), the LUMO energies (E_{LUMO} = −2.35 to −3.11 eV), the HOMO–LUMO gap (ΔE = 2.07–2.66 eV), and the absorption/emission maxima ($\lambda_{max}^{A/E}$ = 442–478/521–678 nm). The experimental data, corroborated by DFT calculations, further revealed twofold and tunable ICT employing both central triphenylamine and auxiliary thiophene donors, and the peripheral F-substitution either boosting or switching-off two-photon absorption activity. Whereas the —SF_5 groups impart an exceptional cross-section of 1930 GM, the —$COCF_3$ group may completely suppress the nonlinear optical response.

1 | Introduction

The last couple of decades has demonstrated triphenylamine (TPA) as a robust electron-donating building block widely utilized in the modular construction of push-pull D-π-A chromophores (D = electron-donor, π = conjugated system and A = electron-acceptor) with numerous applications across optoelectronics [1, 2]. This situation stems from its direct synthetic availability, good electron-donating and transporting capability, hole-transporting properties, and facile functionalization [3]. The propeller-shaped arrangement predisposes TPA to building octupolar chromophores with the centrifugal D-(π-A)$_3$ architecture featuring various π-branches and diverse peripheral electron-acceptors [4]. Due to strong electronic coupling between the individual branches, tripodal TPA chromophores generally possess exceptional hyperpolarizability and a two-photon absorption (2PA) cross-section [3, 5–9] that have been utilized across materials science, biology, and medicine [10–12]. Two-photon fluorescence microscopy [13], 2PA fluorescence cellular imaging [14–17], and photodynamic therapy [18–21] have become routinely employed noninvasive biomedical methods, while microfabrication [22–24], 3D data storage [25, 26], and up-converted lasing [27] represent prominent material applications.

Fluorine is a relatively small atom with the highest electronegativity and low polarizability. It forms a high-energy C—F bond (≈ 480 kJ·mol^{-1}), which is strategically used to improve chemical and thermal stability of (per)fluorinated organic compounds as well as to modulate their biological activity. In this respect, fluorination primarily improves cell permeability, lipophilicity, solubility, and

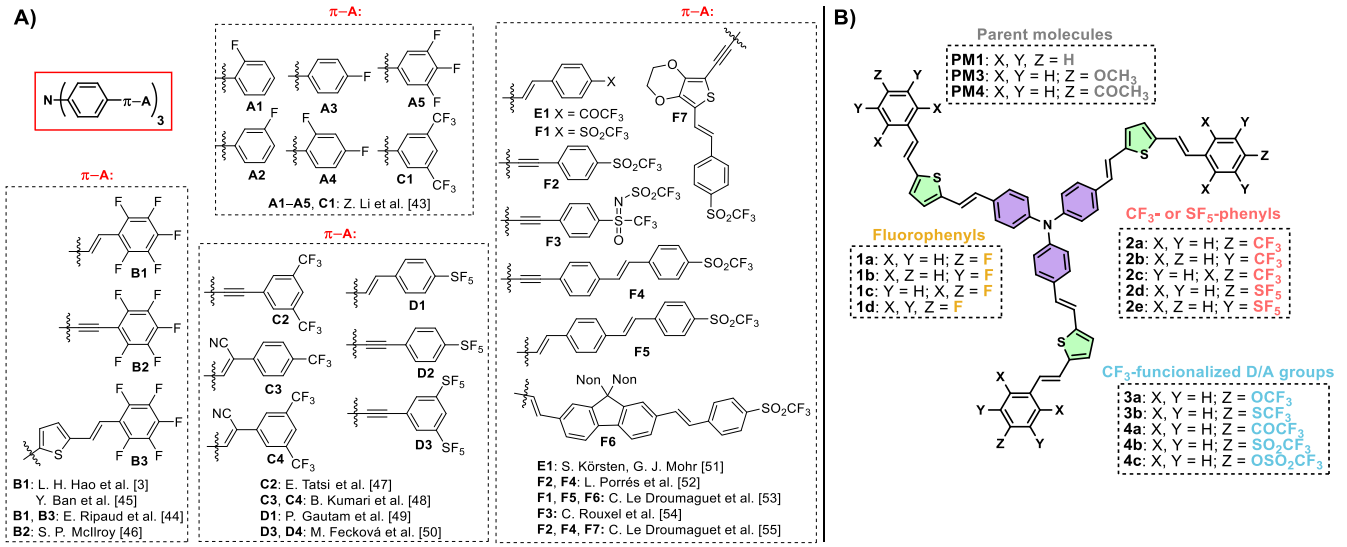

FIGURE 1 | (A) Known tripodal TPA chromophores bearing varied π-system and fluorine-based acceptors; (B) Investigated tripodal TPA-based fluorophores in this work.

other pharmacological parameters [28, 29]. Furthermore, the strongly polarized C—F bond may affect molecular geometry, charge/electron distribution, and specific noncovalent interactions such as C—F•••H hydrogen bonding or π–π^F interactions [30–32]. Appending fluorine atom(s) to a π-conjugated system substantially alters the electronic distribution and allows tuning of the HOMO/LUMO levels and semiconducting properties. Numerous reports have demonstrated enhanced performance and characteristics of fluorinated organic materials over their nonfluorinated analogues [33], for example, pronounced nonlinear optical (NLO) activity [30–32]. Single- (σ_p(F) = 0.06), perfluoro- or trifluoromethyl-substituted (–CF_3; σ_p = 0.35) push-pull systems are among the most widely utilized strategies [28, 29]. In contrast, the octahedral pentafluorosulfanyl [34] (—SF_5; σ_p = 0.68) is much less employed, while the trifluoroacetyl (—$COCF_3$; σ_p = 0.80) is a relatively scarce electron-acceptor [35–37]. Trifluoromethoxy (—OCF_3; σ_p = 0.35), trifluorosulfanyl (—SCF_3; σ_p = 0.50), and trifluoromethyl sulfone (—SO_2CF_3; σ_p = 0.96) are known substituents in agrochemicals or pharmaceuticals [38–40]. The listed Hammett substituent constants (σ_p) allow a rough evaluation of the electronic effects and point out the trifluoromethyl sulfone and trifluoroacetyl as very potent acceptors, superior to the common nitro group (σ_p = 0.78) [41]. While the moderate withdrawing strength of the —CF_3 and —SF_5 substituents stems from negative inductive effects and eventual hyperconjugation, the —$COCF_3$ or —SO_2CF_3 substituents combine negative mesomeric and inductive effects. In addition, the less withdrawing —OCF_3 and —SCF_3 groups oscillate orthogonally to the appended aryl ring, thereby affecting π-conjugation and electron distribution differently from the tetrahedral —CF_3 substituent [38, 42].

Figure 1A summarizes the reported TPA chromophores bearing (poly)fluorinated acceptors **A–F**. Gradually fluorinated benzenes have been used as peripheral acceptors in TPA derivatives **A1–5** and **C1**, which proved useful as blue-violet emitters or hole-transporters of OLEDs [43]. Even better OLED characteristics were measured for pentafluorophenyl derivatives **B1** and **B3**, [44] while **B1** also showed noticeable third-order optical nonlinearity [3, 45]. The pentafluorophenylethynyl pendant in **B2** allowed a substantial singlet oxygen production upon two-photon excitation [46]. Bis(trifluoromethyl) derivative **C2** has been reported as a moderate luminophore for luminescent solar concentrators [47] and CF_3-capped cyanostilbenes **C3–C4** are AIEgens forming stable organogels [48]. The first pentafluorosulfanyl-terminated TPA chromophore **D1**, reported in 2018 by Gautam et al., demonstrated a large 2PA cross-section reaching 2000 GM [49], verifying the SF_5 group as a potent electron-withdrawing unit for efficient multiphoton absorbers. This year, we further demonstrated a selective employment of the electronic effects of the SF_5 group in a series of tripodal fluorophores **D2—D3**. The SF_5 group placed in the *para* position allows hyperconjugation with the TPA donor and imparts **D2** a 2PA cross-section of 600 GM [50]. The trifluoroacetyl-substituted derivative **E1** is capable of sensing amines [51], while the strongly withdrawing trifluoromethyl sulfone has been investigated by the research team of M. Blanchard–Desce [52–55]. Property tuning in **F1—F7** was achieved by altering the π-system, while the olefinic linker turned out to be more efficient as compared to the acetylenic one. When comparing **F4** and **F5**, the latter showed twofold increase in the 2PA activity, reaching 2000 GM. A comparison of the fluorinated sulfone and sulfoximinyl groups in **F2** and **F3** reveals the $SO(NSO_2CF_3)CF_3$ group as "superacceptor" with the σ_p = 1.35 and enhanced 2PA activity (500 vs. 870 GM).

Despite increasing popularity, the current state-of-the-art lacks a systematic study comprehensively comparing fluorine-based substituents and their impact on the fundamental optoelectronic properties of push-pull molecules, while only fragmented and limited reports available to date [56–58]. Hence, based on our continuing interest in octupolar fluorophores with 2PA activity [59–63] and following our recent study on SF_5-terminated TPA fluorophores [50], we present herein an extensive series of C_3-symmetric push-pull molecules **1—4** (Figure 1B). These designed systems feature varying numbers (1–5) of the fluorinated groups at the periphery (—F, —CF_3, —SF_5, —OCF_3, —SCF_3, —$COCF_3$,

—SO_2CF_3, and —OSO_2CF_3) placed at different position along the periphery (*ortho*, *meta*, *para*) to systematically investigate their optoelectronic properties. The central TPA donor and the peripheral acceptors are interconnected via a novel, highly polarizable 2,5-divinylthiophene π-linker possessing thiophene as an auxiliary donor, which is introduced into TPA chromophores for the first time. Both vinylene spacers enforce planarity, assure efficient intramolecular charge transfer (ICT), and, supposedly, also enhance 2PA activity. In addition, we present a series of parent molecules **PM1**–**3** and one linear analogue **2aL** to properly address the effect of fluorination and branching. The fundamental chemical, thermal, electrochemical, photophysical, and (non)linear optical properties of **1**–**4** and **PM1**–**3** were further corroborated by quantum-chemical calculations.

2 | Results and Discussion

2.1 | Synthesis

To synthesize all target fluorophores **PM1**–**3** and **1**–**4** in a straightforward manner, four synthetic steps involving Suzuki-Miyaura cross-coupling (2×), selective bromination, and Heck olefination were employed (Scheme 1C). The substituted iodo- or bromobenzenes **10**–**14** (Scheme 1B) were used to introduce the fluorinated acceptors; intermediates **12c**, **12d**, and **9** were prepared according to the modified literature procedures (see the Supporting Information for more details) [52, 64, 65]. (*E*)-2-(Thiophen-2-yl)ethenylboronic acid pinacol ester **7**, a key intermediate allowing the facile and systematic construction of each branch, was smoothly prepared from 2-bromothiophene **5** and the vinylboronic acid pinacol ester **6** via a Pd-catalyzed Heck olefination in 93% yield (Scheme 1A) [66]. The fluorinated acceptors **10**–**14** were first cross-coupled with the intermediate **7** affording the corresponding phenylethenylthiophenes **15**–**19** in satisfactory yields of ca. 60–90% (Scheme 1C). Selective bromination with NBS furnished the bromothiophenes **20**–**24** (64%–97%), which underwent subsequent Heck olefination with vinylboronic acid pinacol ester **6** under optimized reaction conditions ([$Pd_2(dba)_3$], P(*t*Bu)$_3$, DIPEA, toluene) to give boronic acid pinacol esters **25**–**29** [55–80%; expect **27e** (33%)]. These esters (branches) and tris(4-iodophenyl)amine **9** were finally threefold cross-coupled to furnish the target fluorophores **PM1**–**3** and **1**–**4** (55–70%). Using 4-bromo-*N*,*N*-dimethylaniline **30** allowed the construction of the linear analogue **2aL**, whose X-ray analysis confirmed the exclusive *E*-configuration of both double bonds within the divinylthiophene linker (Figure S1).

2.2 | Thermal Properties

Thermal properties of **PM1**–**3** and **1**–**4** were determined by differential scanning calorimetry, the recorded temperatures of melting T_m, glass transition T_g and thermal decomposition T_d are summarized in Table 1; the native DSC thermograms are provided in the SI. The studied compounds represent large tripodal structures with relatively high molecular weights (876–1632 g·mol^{-1}), which hinder their crystallization and tend them to form amorphous glassy or semicrystalline solids upon precipitation from solution. Consequently, glass transitions of amorphs or broad melting processes of semicrystalline solids were primarily observed upon heating. A sharp endothermic melting, preceded by a cold crystallization at 137 °C, was recorded only for the pentafluorophenyl derivative **1d** at 223 °C. The semicrystalline compounds **PM2**, **1a**, **1c**, **2a**, **2b**, and **3a** underwent broad melting process (111–186 °C), but a reheating cycle was accompanied only by a glass transition, pointing to their complete amorphization. A distinctive and reversible glass transition (T_g = 89–147 °C) without any subsequent melting was observed for the remaining compounds. Whereas the tripodal **2a** showed only an exothermic irreversible peak at around 280 °C, the linear analogue **2aL** melted at 233 °C and exothermically decomposed up to 300 °C. The thermal degradation was generally recorded as either a vigorous or gradual exothermic process, with T_d values ranging from 210 to 420 °C. Sharing the same central TPA donor and the π-system, the differences in thermal behavior are attributed to the peripheral fluoro-acceptors. A rapid decomposition peak was revealed for **1d** (5×F), **2c** (3×CF_3), **2d** (SF_5), **3b** (SCF_3), **4a** ($COCF_3$), and **4c** (OSO_2CF_3), whereas a slow and gradual degradation was seen for molecules **PM1** (H), **PM2** (OCH_3), **1a** (F), **2a** (CF_3), **2b** (2×CF_3), and **4b** (SO_2CF_3). Thermal stability is apparently enhanced by CF_3 groups in the series **2a**–**c** (T_d = 290–420 °C), by the two SF_5 groups in **2e** (T_d = 290 °C), and by the SO_2CF_3 pendants in **4b** (T_d = 340 °C). Consequently, the highest thermal robustness was measured for **2c** (T_d = 420 °C) bearing nine peripheral trifluoromethyl groups.

2.3 | Electrochemistry

The electrochemical behavior of the target fluorophores **PM1**–**3** and **1**–**4** was investigated in THF containing 0.1 M Bu_4NPF_6 using a three-electrode cell by cyclic voltammetry (CV). The acquired electrochemical data are summarized in Table 1, while further experimental details, recorded CV diagrams, and comparison of the tripodal and linear analogues are given in the Supporting Information.

Oxidation was recorded as a multi-electron process consisting of the first reversible one-electron oxidation appearing as a distinguishable shoulder ($E_{1/2(ox1)}$), presumably involving the TPA donor, followed by consecutive irreversible oxidations ($E_{p(ox2)}$) associated with the thiophene auxiliary donors. This electrochemical behavior is consistent with the TPA-(π-Th-π-FluoroA)$_3$ arrangement of the studied tripodal systems. Reduction is a multi-electron process occurring over the peripheral withdrawing groups as well as the adjacent π-system. The (quasi)reversible first reduction ($E_{1/2(red1)}$) was recorded either as a shoulder or as a fully developed peak. However, the SF_5- and F_3CSO_2O-substituted compounds **2d**–**e** and **4c** exhibited fully irreversible first reductions ($E_{p(red1)}$), consistent with our previous observation [50]. The multi-electron transfer is related to the tripodal character and the number of appended fluorine atoms. For instance, incorporating two SF_5 (**2e**) or three CF_3 groups (**2c**) into each branch proportionally increases the number of transferred electrons during the consecutive reductions. The obtained half-wave potentials of the first oxidation and reduction $E_{1/2(ox1/red1)}$ for tripodal **PM1**–**3** and **1**–**4** were found within the range of 0.75 to 0.89 V and −1.21 to −1.89 V, respectively, and were further converted into energy

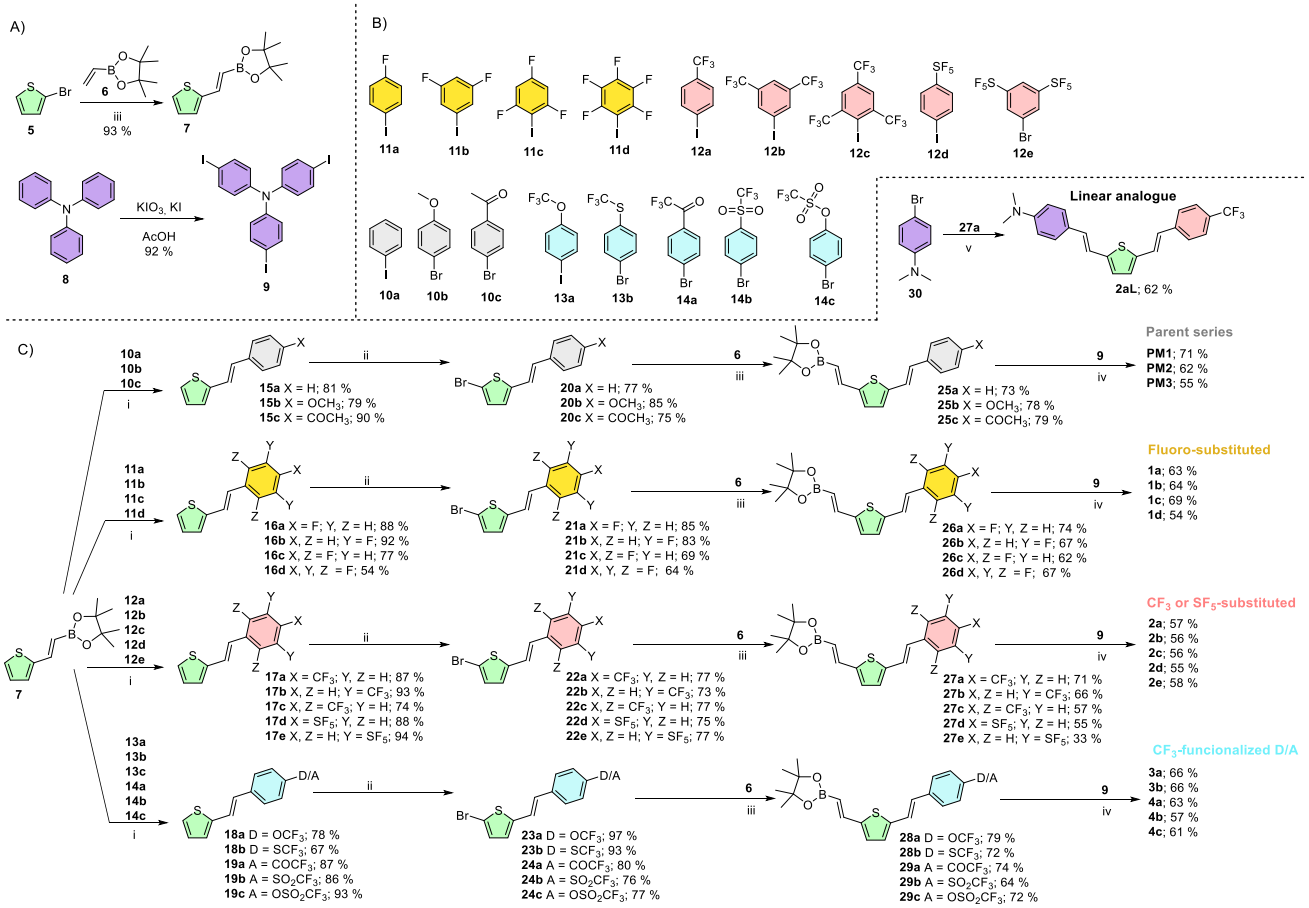

SCHEME 1 | Synthetic pathways towards tripodal fluorophores **1–4**. (A) Synthesis of the key intermediates **7** and **9**. (B) Structures of the starting bromo or iodobenzenes bearing fluoro acceptors. (C) Straightforward four-step reaction pathway towards all target fluorophores **PM1–3** and **1–4**: (i) **7** (1.1 eq), $[PdCl_2(PPh_3)_2]$ (0.02 eq), K_2CO_3 (1.5 eq), THF/H_2O 4:1, 60 °C, 18 h; (ii) NBS (1.05 eq), $CHCl_3$/AcOH 2:1, 80 °C, 18 h; (iii) vinylboronic acid pinacol ester **6** (1.5 eq), $[Pd_2(dba)_3]$ (0.01 eq), P(*t*Bu)$_3$ (0.05 eq), DIPEA (2 eq), toluene, 95 °C, 18 h; (iv) corresponding boronic acid pinacol ester (3.6 eq), $[PdCl_2(PPh_3)_2]$ (0.06 eq), K_2CO_3 (5 eq), THF/H_2O 4:1, 60 °C, 18 h; (v) **27a** (1.1 eq), $[PdCl_2(PPh_3)_2]$ (0.02 eq), K_2CO_3 (1.5 eq), THF/H_2O 4:1, 60 °C, 2 h.

range (eV) in order to experimentally estimate the HOMO/LUMO levels (Table 1). The energy level diagram in Figure 2 visualizes the experimentally estimated HOMO/LUMO energies and electrochemical gaps ΔE^{CV}. Taking the unsubstituted derivative **PM1** as the parent molecule ($E_{HOMO/LUMO}{}^{CV} = -5.11/-2.51$ eV, $\Delta E^{CV} = 2.60$ eV), the HOMO level remains relatively steady across the series and principal changes are seen in the LUMO level upon further substitution. The LUMO is raised/lowered depending on whether an electron donor or acceptor is appended, e.g. **PM2** with a methoxy donor ($E_{LUMO}{}^{CV} = -2.43$ eV) or **PM3** bearing an electron-withdrawing acetyl group ($E_{LUMO}{}^{CV} = -2.70$ eV). Attaching a single fluorine (**1a**), CF_3 (**2a**) or SF_5 (**1d**) into the *para* position gradually decreases the $E_{LUMO}{}^{CV}$ from −2.59 to −2.76 eV as a result of increasing negative inductive effect and eventually employing negative hyperconjugation [70]. Beginning with these mono-substituted derivatives and gradually attaching additional fluorine-containing substituents (**1a→1d**, **2a→2c** or **2d→2e**), the LUMO is further deepened, with the narrowest HOMO–LUMO gap observed for tris(trifluoromethyl) derivative **2c**. Nearly identical HOMO/LUMO levels were measured for the methoxy- and trifluoromethoxy-substituted molecules **PM2** and **3a**, indicating persistent mesomeric electron-donating behavior of both substituents. In contrast, a replacement of the chalcogens (O→S, **3a→3b**) lowers the LUMO energy due to the weaker donating ability of the SCF_3 group. Comparison of the acetyl and trifluoroacetyl derivatives **PM3** and **4a** reveals significantly pronounced electron-withdrawing character of the latter. Hence, compound **4a**, bearing three peripheral $COCF_3$ acceptors, possesses the narrowest HOMO–LUMO gap ($\Delta E^{CV} = 2.07$ eV), whereas the analogous sulfone **4b** was found to be a less effective mesomeric acceptor ($\Delta E_{LUMO}{}^{CV} \sim 0.1$ eV). Contradictorily to **PM2** and **3a**, the trifluoromethyl sulfonate group in **4c** behaves rather as an electron-acceptor and demonstrates electronic effects comparable to the SF_5-group in **2d**. These trends, particularly for the *para*-substituted derivatives, correspond to the Hammett σ_p^- constants [41] as demonstrated by the correlation present in Figure S24, and identify the —SF_5, —SO_2CF_3, and —$COCF_3$ groups as among the most powerful electron-withdrawing substituents within this series.

2.4 | Linear Optical Properties

Chromophores **PM1–3** and **1–4** are intensively orange or red solids, with their fundamental photophysical parameters listed in Tables 2 (THF), S2 (toluene), and S3 (acetonitrile). The absorption

TABLE 1 | Thermal and electrochemical properties of fluorophores **PM1–3** and **1–4**.

	Comp.	T_m [°C][a]	T_g [°C][a]	T_d [°C][b]	$E_{1/2(ox1)}$ [V][c]	$E_{p(ox2)}$ [V][d]	$E_{1/2(red1)}$ [V][c]	ΔE^{CV} [eV][c]	$E_{HOMO}{}^{CV}$ [eV][f]	$E_{LUMO}{}^{CV}$ [eV][f]
Parent series	**PM1**	–	97	250	0.79	1.11	−1.81	2.60	−5.11	−2.51
	PM2	134	100	230	0.77	1.03	−1.89	2.66	−5.09	−2.43
	PM3	–	118	220	0.79	1.08	−1.62	2.41	−5.11	−2.70
Fluoro-subst.	**1a**	154	102	230	0.89	1.23	−1.73	2.62	−5.21	−2.59
	1b	–	92	240	0.88	1.14	−1.64	2.52	−5.20	−2.68
	1c	186	–	250	0.88	1.15	−1.69	2.57	−5.20	−2.63
	1d	223	114	250	0.88	1.15	−1.52	2.40	−5.20	−2.80
CF_3- and SF_5-subst.	**2a**	183	112	310	0.83	1.08	−1.68	2.51	−5.15	−2.64
	2aL	233	–	300	0.50	0.79	−1.97[e]	2.47	−4.82	−2.35
	2b	120	107	290	0.81	1.08	−1.64	2.45	−5.13	−2.68
	2c	–	–	420	0.82	1.10	−1.42	2.24	−5.14	−2.90
	2d	–	135	230	0.82	1.09	−1.56[e]	2.38	−5.14	−2.76
	2e	–	–	290	0.86	1.10	−1.45[e]	2.31	−5.18	−2.87
CF_3-funcional. D/A	**3a**	111	89	220	0.75	1.08	−1.84	2.59	−5.07	−2.48
	3b	–	92	230	0.76	1.05	−1.72	2.48	−5.08	−2.60
	4a	–	110	210	0.86	1.12	−1.21	2.07	−5.18	−3.11
	4b	–	147	340	0.87	1.14	−1.30	2.17	−5.19	−3.02
	4c	–	100	230	0.85	1.13	−1.59[e]	2.44	−5.17	−2.73

[a] T_m = temperature of melting, T_g = temperature of glass transition (the point of intersection of a baseline and a tangent of DSC peak/step = onset).
[b] T_d = thermal decomposition (pyrolysis in N_2 atmosphere).
[c] $E_{1/2(ox1)}$ and $E_{1/2(red1)}$ are half-wave potentials of the first oxidation and reduction, respectively, as measured by CV in THF containing 0.1 M Bu_4NPF_6; all potentials are given *vs.* SSCE, $\Delta E^{CV} = E_{1/2(ox1)} - E_{1/2(red1)}$.
[d] $E_{p(ox2)}$ is peak potential of the irreversible second (subsequent) oxidation.
[e] Fully irreversible first reduction ($E_p{}^c$ value).
[f] Experimentally deduced $E_{HOMO}{}^{CV}$ and $E_{LUMO}{}^{CV}$: $-E_{HOMO/LUMO}{}^{CV} = (E_{1/2(ox1)} + 0.036)$ or $(E_{1/2(red1)} + 0.036) + 4.28$ (vs. SCE) [67, 68]. The increment of +0.036 V corresponds to the difference between SCE (0.241 vs. SHE) and SSCE (0.205 vs. SHE)) [69].

and emission spectra of representative **PM1**, **1a**, **2a**, and **2d** in THF are shown in Figure 3. Based on the Frenkel exciton model [8], three excited states are generally predicted for C_3-symmetric tripodal chromophores. However, the two low-energy states (relative to the corresponding linear chromophore) are expected to be degenerate, while the high-energy state possesses zero oscillator strength. Consequently, the absorption spectra of tripodal chromophores typically appear as a single band corresponding to that of the linear analogue [50, 73]. Fluorophores **PM1–3** and **1–4** exhibit a single absorption band (Figures S25–29), accompanied by a high-energy shoulder at around 360 nm. When comparing the linear **2aL** ($\lambda_{max}{}^{A/E}$ = 429/583 nm) with the tripodal **2a** ($\lambda_{max}{}^{A/E}$ = 450/563 nm), both absorption and emission spectra are nearly identical (Figure S30), supporting the aforementioned assumption. The longest-wavelength absorption maxima of the tripodal fluorophores **PM1–3** and **1–4** lie between 442 and 478 nm, with molar absorption coefficients in the range of 105–180×10^3 $M^{-1}cm^{-1}$. This contrasts with the linear derivative **2aL** (ε_{max} = 55.6 ×10^3 $M^{-1}cm^{-1}$). Thus, increasing the number of chromophoric units enhances the absorption, which is a typical feature of linear vs. tripodal systems [73]. In agreement with the electrochemical measurements, the observed red/blue shifts in the absorption maxima arise from structural variations in the fluorine-based peripheral substituents. The same trends are obeyed as can be demonstrated by a tight correlation of the optical ($1240/\lambda_{max}{}^{A}$) and electrochemical gaps (ΔE), see Figures S35 in the Supporting Information. Fluorophore **2c** features different photophysical behavior, including blue-shifted absorption maxima, substantially quenched fluorescence in THF, the most red-shifted emission band in toluene, and intense solid-state emission. This behavior is likely associated with a nonplanar arrangement of the terminal phenyl ring caused by *ortho*-substitution with bulky CF_3-groups [74]. The most red-shifted CT bands were recorded for **4a** and **4b** (478 and 473 nm), bearing —$COCF_3$ and —SO_2CF_3 powerful acceptors. Only minor solvatochromism was detected in the absorption spectra (Figure S31–34), which is a typical feature of push–pull chromophores [75].

The target molecules showed a single broad emission band in THF and ACN, while an apparent low-energy shoulder was recorded in nonpolar toluene due to vibronic transitions commonly found in nonpolar media [76]. Compared to the absorption spectra, the emission maxima of **PM1–3** and **1–4** span a broad

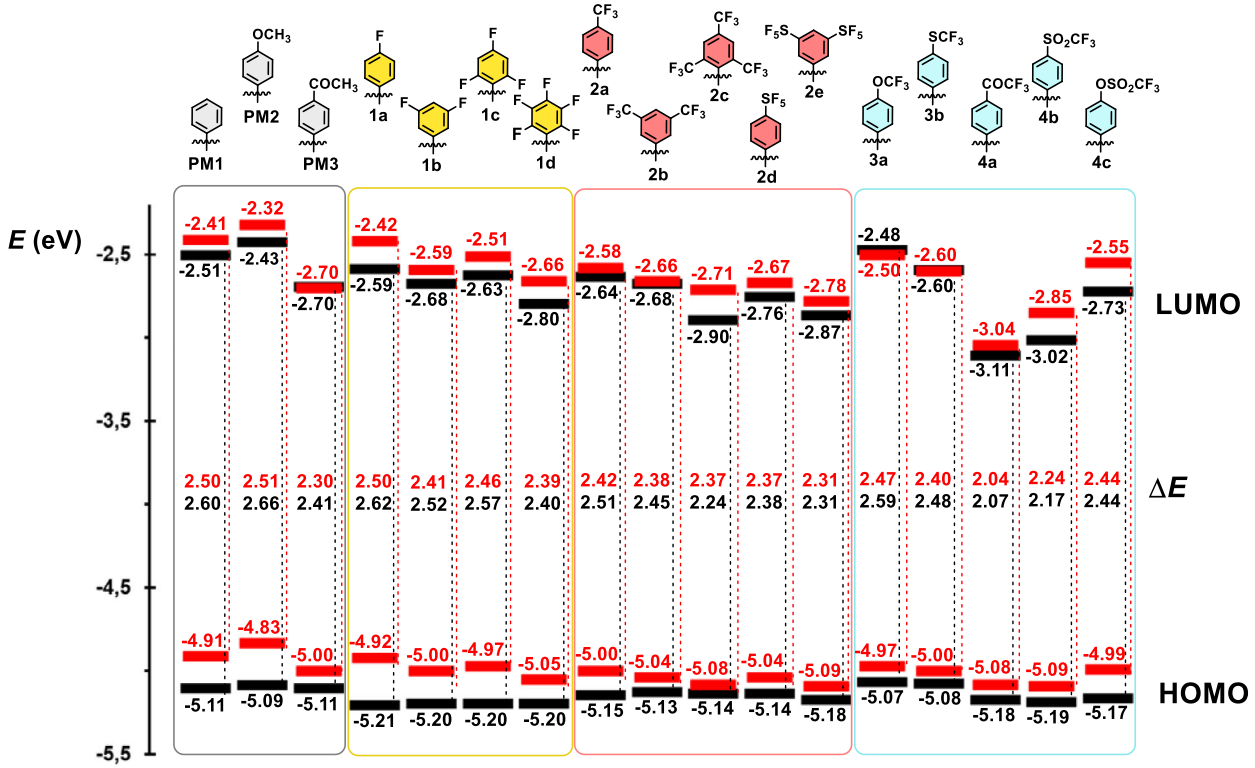

FIGURE 2 | Energy level diagram of the electrochemically estimated (black) and the DFT-calculated (red) HOMO/LUMO values for fluorophores **PM1–3** and **1–4**.

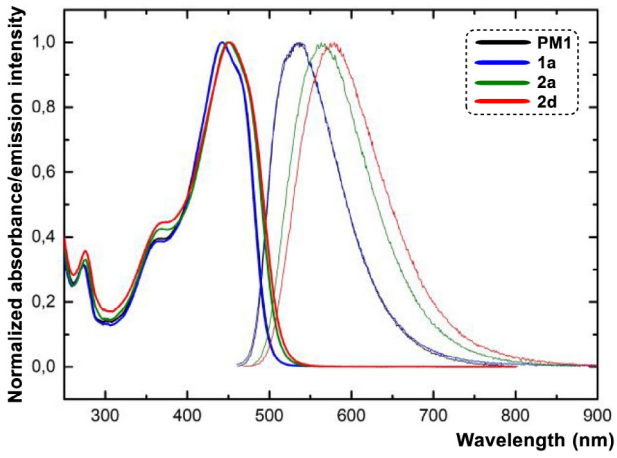

FIGURE 3 | Normalized UV-Vis absorption (bold line) and emission spectra (thin line) of fluorophores **PM1** (4-H), **1a** (4-F), **2a** (4-CF_3), and **2d** (4-SF_5) measured in THF ($c \approx 5\times10^{-6}$ M).

range (521 to 678 nm) and are obviously much more influenced by the structural aspects, similarly to the aforementioned electrochemical data (see Figure S36 for the correlation). This implies a greater polarization/stabilization of the excited state, arising from considerable structural/geometrical reorganization compared to the ground state. As expected, this effect is most pronounced for the nonplanar **2c**, which showed the largest Stokes shift above 6100 cm^{-1} in toluene (Table S2). In general, the emission maximum shifts bathochromically with an increasing number of fluorine atoms/fluorine-based substituents or upon replacing CH_3 by CF_3 groups. A positive solvatochromism observed in more polar solvents (ACN) further confirms the polar nature of the excited state, however, the stabilization is accompanied by a diminished fluorescence intensity. In THF, the fluorescence quantum yields (Φ^F) range within a narrow interval of 0.36–0.56 and decrease significantly upon attaching powerful withdrawing substituents (−$COCF_3$ and −SO_2CF_3), which enhance ICT, as in **4a–b** (Φ^F = 0.06–0.11). A similarly narrow range of Φ^F values (0.44–0.54) was found in toluene. The excited states of **PM1–3** and **1–4** were further studied by fluorescence-decay measurements in toluene and THF (Figures 4 and S37–46 and Tables 2 and S4,S5). The average fluorescence lifetimes τ range from 0.3 to 2.2 ns (THF, Table 2) and depend on both structural changes and solvent polarity. Figure 4 presents the decay profiles for the representative fluorophores **PM1**, **1a**, **2a**, and **2d** in toluene and THF showing extended lifetimes for chromophores with a larger number of fluorine atoms and fluorine-based substituents. On the contrary, replacing CH_3 by CF_3 in the acetyl group (**PM3→4a**) results in a substantial decrease in the lifetime (1.9→0.34 ns), while it increases again for **4b** (0.64 ns, −SO_2CF_3) and **4c** (1.83 ns, −OSO_2CF_3). However, **4a–c** exhibited even longer lifetimes in toluene than the parent systems **PM2**/**3** (Table S5).

Fluorophores **PM3**, **2c**, **2e**, and **4b**, all bearing powerful withdrawing termini, also showed a noticeable solid-state emission (Table 2, Figures S47–48). Compared to their solution emissions, the solid-state emission spectra are red-shifted and display low-energy shoulders, indicating significant intermolecular interactions and possible formation of excimers [77]. Fluorophore **2c** exhibits the strongest solid-state intensity, attributed to the *ortho*-oriented CF_3-groups, which affect molecular packing in the solid

TABLE 2 | Linear and nonlinear optical data of fluorophores **PM1–3** and **1–4** in THF.

Comp.		Solution							Powder
		$\lambda_{max}{}^{A}$ [nm/eV][a]	$\varepsilon_{max}{}^{A}$ [10^3 $M^{-1}cm^{-1}$][a]	$\lambda_{max}{}^{E}$ [nm/eV][a]	<τ> [ns][a]	Φ^{F} [-][b]	Stokes shift [cm^{-1}/eV]	$\delta_{2PA}/\lambda_{2PA}$ [GM/nm][c]	$\lambda_{max}{}^{E}$ [nm][d]
Parent series	**PM1**	443/2.80	181	535/2.32	1.61	0.50	3880/0.48	890/740	[f]
	PM2	443/2.80	159	521/2.38	1.39	0.56	3380/0.42	850/740	[f]
	PM3	456/2.72	110	585/2.12	1.90	0.47	4840/0.60	550/730	650
Fluoro-subst.	**1a**	442/2.81	134	535/2.32	1.65	0.46	3900/0.49	910/740	[f]
	1b	448/2.77	117	562/2.21	1.93	0.49	4530/0.56	800/740	[f]
	1c	446/2.78	105	550/2.25	1.92	0.54	4240/0.53	610/740	[f]
	1d	457/2.71	146	587/2.11	2.23	0.52	4850/0.60	810/740	[f]
CF_3- and SF_5-subst.	**2a**	450/2.76	130	563/2.20	1.91	0.49	4460/0.55	670/740	[f]
	2aL	429/2.89	55.6	583/2.13	[h]	[h]	6160/0.76	[h]	[f]
	2b	453/2.74	119	583/2.13	2.06	0.48	4920/0.61	560/740	[f]
	2c	443/2.80	175	[e]	0.32	[e]	[e]	[g]	622
	2d	452/2.74	138	578/2.15	1.94	0.45	4820/0.60	530/740	[f]
	2e	458/2.71	120	603/2.06	1.90	0.36	5250/0.65	1930/740	617
CF_3-funcion. D/A	**3a**	444/2.79	129	545/2.28	1.76	0.48	4170/0.52	1250/740	[f]
	3b	452/2.74	118	568/2.18	1.87	0.49	4520/0.56	780/750	[f]
	4a	478/2.59	163	678/1.83	0.34	0.06	6170/0.77	[g]	[f]
	4b	473/2.62	124	665/1.86	0.64	0.11	6100/0.76	1170/730	710
	4c	447/2.77	134	553/2.24	1.83	0.49	4290/0.53	710/740	[f]

[a]Measured in THF (Dimroth–Reichardt polarity parameter $E_T^N = 0.207$ [71]) at concentration ≈ 5×10^{-6} M; emitted at the absorption maximum wavelength.
[b]Fluorescence quantum yield (±10%) determined relative to perylene as a standard ($\Phi^{F} = 0.94$ in cyclohexane) [72].
[c]Measured in THF.
[d]Emitted at the absorption maximum wavelength determined in THF solution.
[e]Non-emissive in THF.
[f]Low intensity of emission in solid state.
[g]Low 2PA excitation fluorescence signal.
[h]Not measured.

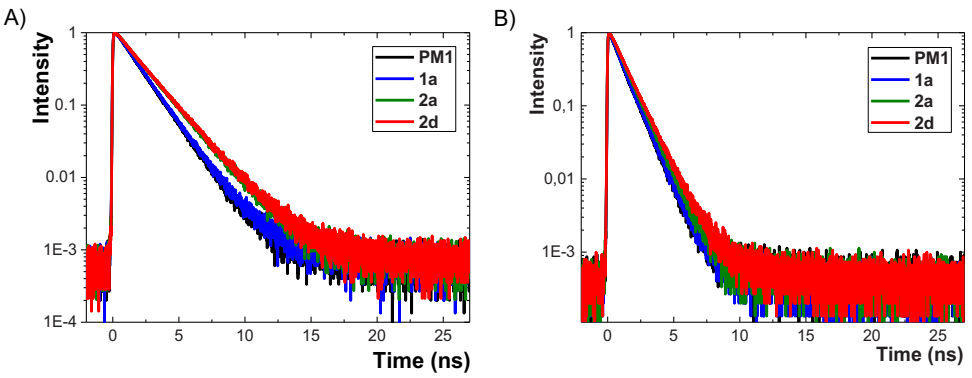

FIGURE 4 | Fluorescence decays in the ns timescale for fluorophores **PM1** (4-H), **1a** (4-F), **2a** (4-CF_3), and **2d** (4-SF_5) measured in A) THF and B) toluene ($c \approx 5\times10^{-6}$ M).

TABLE 3 | The DFT calculated data of fluorophores **PM1–3** and **1–4**.

	Comp.	E_{HOMO}^{DFT} [eV][a]	$E_{HOMO-1(-2)}^{DFT}$ [eV][a]	$E_{LUMO(+1)}^{DFT}$ [eV][a]	E_{LUMO+2}^{DFT} [eV][a]	ΔE^{DFT} [eV][a]	μ_g^{DFT} (D)[a]	λ_{max}^{DFT} (nm/eV)[b]	λ_{max}^{DFT} (nm/eV)[c]
Parent series	**PM1**	−4.91	−5.40	−2.41	−2.20	2.50	1.4	577/2.15	451/2.75
	PM2	−4.83	−5.24	−2.32	−2.10	2.51	2.6	575/2.16	454/2.73
	PM3	−5.00	−5.53	−2.70	−2.57	2.30	0.8	623/1.99	467/2.66
Fluoro-subst.	**1a**	−4.92	−5.41	−2.42	−2.22	2.50	3.4	576/2.15	462/2.68
	1b	−5.00	−5.54	−2.59	−2.40	2.41	4.6	550/2.25	430/2.88
	1c	−4.97	−5.50	−2.51	−2.32	2.46	2.6	572/2.17	446/2.78
	1d	−5.05	−5.62	−2.66	−2.49	2.39	5.6	583/2.13	446/2.78
CF_3- and SF_5-subst.	**2a**	−5.00	−5.54	−2.58	−2.41	2.42	9.4	598/2.07	459/2.70
	2aL	−4.98	−5.96(−7.01)	−2.38(−1.25)	−0.84	2.60	10.9	534/2.32	448.2.77
	2b	−5.04	−5.61	−2.66	−2.50	2.38	9.0	593/2.09	451/2.75
	2c	−5.08	−5.72	−2.71	−2.58	2.37	4.6	608/2.04	–[d]
	2d	−5.04	−5.60	−2.67	−2.51	2.37	9.2	600/2.07	453/2.74
	2e	−5.09	−5.69	−2.78	−2.64	2.31	10.5	623/1.99	465/2.67
CF_3-funcional. D/A	**3a**	−4.97	−5.49	−2.50	−2.31	2.47	3.5	587/2.11	455/2.73
	3b	−5.00	−5.54	−2.60	−2.44	2.40	8.6	596/2.08	456/2.72
	4a	−5.08	−5.63	−3.04	−2.96	2.04	10.5	698/1.78	488/2.54
	4b	−5.09	−5.67	−2.85	−2.73	2.24	13.3	621/2.00	456/2.72
	4c	−4.99	−5.51	−2.55	−2.36	2.44	3.8	572/2.17	441/2.81

[a]Calculated using the DFT B3LYP/6−311+G(2d,p) level in THF.
[b]Calculated using the TD-DFT (nstates = 8) B3LYP/6−311++G(2d,p) level in THF.
[c]Calculated using the TD-DFT (nstates = 8) CAM-B3LYP/6−311++G(2d,p) level in THF.
[d]Calculation failed.

state [78]. The nonplanar arrangement restricts an intramolecular rotation and opens aggregation-induced emission [74].

2.5 | Theoretical DFT Calculations

The spatial, electronic and optical properties of the target fluorophores **PM1–3** and **1–4** were further predicted using DFT methods implemented in Gaussian16 W software package [79]. The initial geometries, frontier molecular orbital energies, and ground-state dipole moments μ_g^{DFT} were optimized/calculated by the DFT B3LYP/6−311+G(2d,p) method in THF (Table 3). Theoretical electronic absorption spectra were calculated at the TD-DFT (nstates = 8) level using both B3LYP/6-311++G(2d,p) and CAM-B3LYP/6-311++G(2d,p) functionals in THF, and the corresponding λ_{max}^{DFT} values were extracted for both methods, see the Supporting Information for more details. The optimized geometry of the representative fluorophore **1d** (Figure 5A) reveals completely planar branches appended to the propeller-shaped TPA, this structural feature is consistent across other molecules in the series. However, it contrasts with the twisted terminal phenyls (dihedral angle ∼ 50 °) of **2c** bearing the bulky trifluoromethyl groups. This geometrical distinction further supports our aforementioned conclusions drawn from the experimental photophysical data. For a comparison between the tripodal and linear analogues **2a**/**2aL**, see the Supporting Information.

The calculated HOMO and LUMO energies $E_{HOMO/LUMO}^{DFT}$ (Figure 2) follow the same trends as seen by the CV measurements, and the calculated E_{LUMO}^{DFT} and HOMO–LUMO gaps correlate tightly with the experimental values (Figures S50–S51). As a general trend, the steady HOMO and the varied LUMO were observed upon changing the terminal fluorine-based substituents. Nearly identical energies were calculated for the HOMO−1/−2 and the LUMO/+1, indicating these pairs of FMOs to be degenerate (Figure 5B), which is in accordance with previous observations [50, 80].

Visualization of the FMOs in the representative chromophore **2a** (Figure 5B; see also Figures S52–S60 for other derivatives) shows that the HOMO is localized on the central TPA unit, while the HOMO−1 is spread over the auxiliary thiophene donor and the adjacent π-system of one branch. The degenerate HOMO−2 displays an analogous distribution over the remaining two branches. The unoccupied orbitals display heterogenous distributions depending on the electron-withdrawing strength of the given acceptor. Fluorophores with weak or absent acceptors possess the LUMO+2 spread over both the thiophene and the adjacent π-system across all three branches (except **2c**). Increasing acceptor

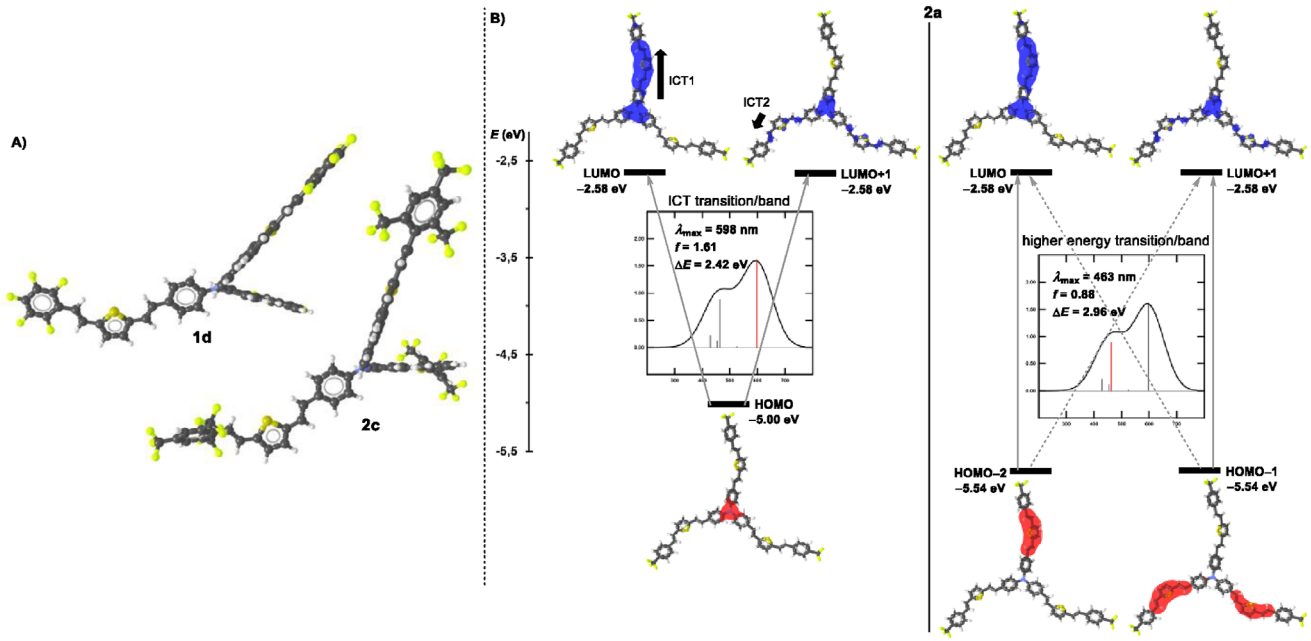

FIGURE 5 | (A) Optimized geometries of fluorophores **1d** and **2c** calculated using DFT B3LYP/6-311+G(2d,p) level; color of atoms: carbon—black, hydrogen—white, nitrogen—blue, sulfur—yellow, fluorine—yellow-green. (B) The principal electron transitions, FMOs and DFT-calculated parameters of the representative trifluoromethyl derivative **2a** [the HOMO(−1,−2) are shown in red, the LUMO(+1,+2) in blue; the vertical lines in the calculated absorption spectra represent oscillator strengths (f)].

character shifts LUMO+2 toward the terminal phenyls (**2b**–**e**) or directly onto the mesomeric acceptors (**PM3**, **4a**–**b**). The LUMO+1 is transitioned from the central TPA donor (**PM2**, **1a**, **2a**, and **3b**) to individual arm (**PM1**, **1b**–**c**, **2d**–**e**, and **3a** or **1d**, **2b**, **2c**, and **4c**) and finally to the terminal strong acceptors (**PM3**, **4a**, **4b**), depending on withdrawing strength. The LUMO itself exhibits a nearly identical distribution as the degenerate LUMO+1 across the second (or third) branch(es), a such splitting is a typical feature of tripodal D(–π–A)$_3$ scaffolds [61]. Hence, the degree of charge separation in the studied molecules can be effectively tuned by varying the electron-withdrawing ability of the terminal substituents.

The UV-Vis absorption spectra of target fluorophores **PM1**–**3** and **1**–**4** were predicted using two different functionals, namely B3LYP and CAM-B3LYP in THF (Table 3 and Figures S61–S68). While the CAM-B3LYP-calculated spectra align well with the experimental bands, the B3LYP-derived spectra obey the shape of the experimental ones but are shifted bathochromically. However, when correlating the experimental and theoretical λ_{max} values, the CAM-B3LYP-derived longest-wavelength absorption maxima showed no meaningful correlation, whereas the B3LYP-calculated data fit well with the experimental values (Figure S69), including the high-energy shoulder. Transition analysis (Figure 5B) revealed that the longest-wavelength band (534–698 nm) originates from two principal transitions: HOMO → LUMO or HOMO → degenerate LUMO+1, both exhibiting the same oscillator strength. The high-energy band arises from four transitions between the degenerate HOMO−1/HOMO−2 to the degenerate LUMO/LUMO+1. All these transitions possess the same oscillator strengths (roughly half those responsible for the CT-band), correspond well to the experimental data, and are largely neglected by the CAM-B3LYP functional. Altogether, the DFT predicted outcomes are in line with the TPA-(π-Th-π-FluoroA)$_3$ structural arrangement, exhibiting two principal ICTs originating from both the TPA and thiophene donors (Figure 5B).

2.6 | Two-Photon Absorption Properties

With respect to their adjustable ICT character and tripodal arrangement, the two-photon absorption properties of **PM1**–**3** and **1**–**4** were further examined by a two-photon excited fluorescence (TPEF) method in THF and toluene (Tables 2 and S2 and Figures 6 and S70–S79). Except **2c** and **4a**, the investigated fluorophores generally exhibited good to excellent 2PA performance, with 2PA cross sections around 1000 GM. When going from the unsubstituted derivative **PM1** to the monofluoro-substituted derivative **1a**, the peak 2PA cross-section at 740 nm in THF slightly increases from 890 to 910 GM; however, the effect is far more pronounced in toluene (1380 GM at 750 nm). Further addition of the fluorine atoms (**1a**→**1d**) did not improve the 2PA activity. Attaching the trifluoromethyl along with the *para*-pentafluorosulfanyl substituents proved rather detrimental, whereas the introduction of two *meta*-positioned SF_5 groups together with the polarizable branches in **2e** yields an exceptional 2PA cross-section of 1930 GM in THF (Table 2). When comparing **2e** to structurally related chromophores, bearing olefinic [49] and acetylenic units [50] and possessing markedly different cross-sections of around 2000 and 500 GM, the influence of a planar chromophoric unit and a cumulation effect of two SF_5 groups must be highlighted. Further increasing the ICT by employing strong mesomeric acceptors such as $COCF_3$ (**4a**) results in a dramatic drop of the TPEF signal, falling below a detectable limit, whereas the trifluoromethyl sulfone derivative **4b** still displayed a noticeable cross-section of 1170 GM. Interestingly, derivative

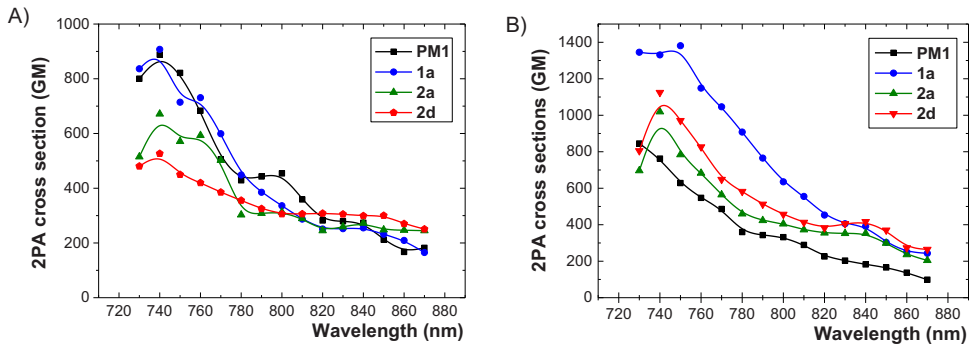

FIGURE 6 | Two-photon absorption spectra for fluorophores **PM1** (4-H), **1a** (4-F), **2a** (4-CF_3), and **2d** (4-SF_5) measured in (A) THF and (B) toluene.

3a, bearing three pseudo-donating OCF_3 groups, exhibited an enhanced δ_{2PA} of 1250 GM, surpassing the 850 GM observed for its methoxy-substituted analogue **PM2**. This further demonstrates that balancing the D/A behavior of the OCF_3 group through a combination of −I and +M effects may represent a viable strategy for increasing two-photon activity. Our TPEF measurements clearly show that a pronounced ICT tends to suppress the two-photon absorption cross-section, particularly in non-polar solvents where stabilization of radiative ICT states is diminished. Chromophores with strong mesomeric acceptors (**PM3**, **4a**, **4b**) show the lowest 2PA cross-sections in toluene, whereas analogues containing none/moderate acceptors (**PM1**−**PM2**, **1a**, **2a**, **2d, 3a**−**b**) maintain higher radiative efficiency, despite lacking octopolar features. Hence, the structural arrangement $(D(-\pi-A)_3$ or $D(-\pi-D)_3$, planarization and composition of the chromophoric units, properly adjusting the extent of ICT, and selecting an appropriate environment seem to be proper tools to design organic absorbers with admirable 2PA activity. Considering the whole portfolio of studied fluorine-based peripheral moieties, the 3,5-diSF_5-substituted chromophore **2e** stands out as particularly exceptional.

3 | Conclusion

Starting from the central TPA donor, we constructed a comprehensive series of propeller-shaped, C_3-symmetric tripodal push–pull fluorophores by linking polarizable 2,5-divinylthiophene units with peripheral fluorinated phenyl rings acting as weak-to-strong electron acceptors. In addition to the tripodal push-pull chromophores **1**−**4**, the series was complemented by one linear (**2aL**) and three non-fluorinated parent compounds (**PM1**−**3**), allowing a thorough comparison across the entire library. The systematic structural variation allowed controlled modulation of the intramolecular charge-transfer (ICT) character, providing a platform to evaluate how subtle changes in the degree of fluorination affect the linear and nonlinear photophysical properties. The target fluorophores were obtained as orange-to-red amorphous or semicrystalline solids with high solubility in solvents of medium and low polarity and with distinct glass transitions or melting processes, reflecting their amorphous or semicrystalline nature. Thermal stability was generally high, with the −CF_3 and −SO_2CF_3-functionalized derivatives **2a**−**c** and **4b** displaying the greatest robustness. In general, peripheral F-functionalization can greatly enhance thermal stability. Electrochemical measurements revealed relatively steady HOMO localized at the central TPA unit, while the LUMO energies were strongly modulated by the electron-withdrawing strength of the peripheral substituents. According to the LUMO energies, the electron withdrawing power of the investigated (per)fluoro groups follows the order: $OCF_3 \approx H < -SCF_3 \approx -F < -CF_3 < -SF_5 \approx -OSO_2CF_3 < -SO_2CF_3 < -COCF_3$. Thus, the trifluoromethoxy group acts as an electronically neutral substituent, whereas the trifluoroacetyl proved to be a highly potent electron acceptor. The steady-state absorption spectra were largely insensitive to structural variations, whereas the emission properties exhibited a strong dependence on the extent of ICT and solvent polarity, with emission maxima tunable from 521 to 678 nm in THF and fluorescence lifetimes ranging from 0.3 to 2.2 ns. Hence, a radiative relaxation can be effectively controlled through the peripheral substitution. The twisted arrangement of the *ortho*-oriented CF_3 groups in **2c** imparts different photophysics in solution and enhanced solid-state fluorescence, further illustrating the critical role of substituent orientation. The experimentally measured two-photon absorption cross-sections ranged from 500 to 1300 GM in THF and toluene, while fluorophore **2e**, bearing two meta-positioned −SF_5 groups, demonstrated an exceptional 2PA cross-section of 1930 GM. In contrast, the two-photon activity of the trifluoroacetyl derivative **4a** was nearly zero in THF. Thus, taking the steady central donor and the conjugated system, the peripheral F-substitution can either boost or quench the NLO activity through controlling the extent of ICT. These results demonstrate that the interplay between the polarizability of the particular chromophoric units, the substituent electronic nature, and the molecular symmetry is crucial for enabling efficient two-photon transitions. This study establishes general principles showing that a careful selection and positioning of the F-substituents can finely modulate ICT and tailor both linear and nonlinear photophysical properties of TPA-centered tripodal fluorophores with perspective applications across 2PA bioimaging, optical data storage, and other nonlinear photonic technologies, where a precise control over the ICT and the two-photon response is essential.

Acknowledgments

This work has been funded by a grant from the Programme Johannes Amos Comenius under the Ministry of Education, Youth and Sports of the Czech Republic [No. CZ.02.01.01/00/23_021/0008593].

Open access publishing facilitated by Univerzita Pardubice, as part of the Wiley - CzechELib agreement.

Conflicts of Interest

The authors declare no conflict of interest.

Data Availability Statement

The data that support the findings of this study are openly available in Figshare at https://doi.org/10.6084/m9.figshare.30646283, reference number 30646283.

References

1. P. Blanchard, C. Malacrida, C. Cabanetos, J. Roncali, and S. Ludwigs, "Triphenylamine and Some of Its Derivatives as Versatile Building Blocks for Organic Electronic Applications," *Polymer International* 68 (2019): 589–606, https://doi.org/10.1002/pi.5695.

2. X. Lian, Z. Zhao, and D. Cheng, "Recent Progress on Triphenylamine Materials: Synthesis, Properties, and Applications," *Molecular Crystals and Liquid Crystals* 648 (2017): 223–235, https://doi.org/10.1080/15421406.2017.1302042.

3. L. H. Hao, E. D. Dai, Y. Q. Ban, et al., "Strong Nonlinear Optical Response in Star-Shaped Push–Pull Triphenylamine Derivatives," *Indian Journal of Physics* 99 (2025): 2627, https://doi.org/10.1007/s12648-024-03492-x.

4. M. Klikar, P. Solanke, J. Tydlitát, and F. Bureš, "Alphabet-Inspired Design of (Hetero)Aromatic Push–Pull Chromophores," *Chemical Record* 16 (2016): 1886, https://doi.org/10.1002/tcr.201600032.

5. D. Beljonne, W. Wenseleers, E. Zojer, et al., "Role of Dimensionality on the Two-Photon Absorption Response of Conjugated Molecules: The Case of Octupolar Compounds," *Advanced Functional Materials* 12 (2002): 631–641, https://doi.org/10.1002/1616-3028(20020916)12:9%3c631::AID-ADFM631%3e3.0.CO;2-W.

6. X. Wang, P. Yang, G. Xu, W. Jiang, and T. Yang, "Two-Photon Absorption and Two-Photon Excited Fluorescence of Triphenylamine-Based Multibranched Chromophores," *Synthetic Metals* 155 (2005): 464–473, https://doi.org/10.1016/j.synthmet.2005.06.006.

7. Y. Gong, G. L. Hou, X. Bi, et al., "Enhanced Two-Photon Absorption in Two Triphenylamine-Based All-Organic Compounds," *Journal of Physical Chemistry A* 125 (2021): 1870–1879, https://doi.org/10.1021/acs.jpca.0c10567.

8. C. Katan, F. Terenziani, O. Mongin, et al., "Effects of (Multi)Branching of Dipolar Chromophores on Photophysical Properties and Two-Photon Absorption," *Journal of Physical Chemistry A* 109 (2005): 3024–3037, https://doi.org/10.1021/jp044193e.

9. H. M. Kim and B. R. Cho, "Two-Photon Materials with Large Two-Photon Cross Sections. Structure-Property Relationship," *Chemical Communications* (2009): 153, https://doi.org/10.1039/B813280A.

10. T. C. Lin, S. J. Chung, K. S. Kim, et al. *Polymers for Photonics Applications II* (Berlin, Heidelberg: Springer Berlin Heidelberg, 2003): 157–193.

11. M. Pawlicki, H. A. Collins, R. G. Denning, and H. L. Anderson, "Two-Photon Absorption and the Design of Two-Photon Dyes," *Angewandte Chemie International Edition* 48 (2009): 3244–3266, https://doi.org/10.1002/anie.200805257.

12. F. Terenziani, C. Katan, E. Badaeva, S. Tretiak, and M. Blanchara-Desce, "Enhanced Two-Photon Absorption of Organic Chromophores: Theoretical and Experimental Assessments," *Advanced Materials* 20 (2008): 4641–4678, https://doi.org/10.1002/adma.200800402.

13. I. Kaminer, J. Nemirovsky, and M. Segev, "Optimizing 3D Multiphoton Fluorescence Microscopy," *Optics Letters* 38 (2013): 3945, https://doi.org/10.1364/OL.38.003945.

14. S. Yao and K. D. Belfield, "Two-Photon Fluorescent Probes for Bioimaging," *European Journal of Organic Chemistry* 2012 (2012): 3199–3217, https://doi.org/10.1002/ejoc.201200281.

15. H. M. Kim and B. R. Cho, "Small-Molecule Two-Photon Probes for Bioimaging Applications," *Chemical Reviews* 115 (2015): 5014–5055, https://doi.org/10.1021/cr5004425.

16. W. Niu, L. Guo, Y. Li, S. Shuang, C. Dong, and M. S. Wong, "Highly Selective Two-Photon Fluorescent Probe for Ratiometric Sensing and Imaging Cysteine in Mitochondria," *Analytical Chemistry* 88 (2016): 1908–1914, https://doi.org/10.1021/acs.analchem.5b04329.

17. H. M. Kim and B. R. Cho, "Two-Photon Probes for Intracellular Free Metal Ions, Acidic Vesicles, and Lipid Rafts in Live Tissues," *Accounts of Chemical Research* 42 (2009): 863–872, https://doi.org/10.1021/ar800185u.

18. G. Chen, I. Roy, C. Yang, and P. N. Prasad, "Nanochemistry and Nanomedicine for Nanoparticle-Based Diagnostics and Therapy," *Chemical Reviews* 116 (2016): 2826–2885, https://doi.org/10.1021/acs.chemrev.5b00148.

19. F. Hammerer, G. Garcia, S. Chen, et al., "Synthesis and Characterization of Glycoconjugated Porphyrin Triphenylamine Hybrids for Targeted Two-Photon Photodynamic Therapy," *The Journal of Organic Chemistry* 79 (2014): 1406–1417, https://doi.org/10.1021/jo402658h.

20. M. Gary-Bobo, Y. Mir, C. Rouxel, et al., "Mannose-Functionalized Mesoporous Silica Nanoparticles for Efficient Two-Photon Photodynamic Therapy of Solid Tumors," *Angewandte Chemie International Edition* 50 (2011): 11425–11429, https://doi.org/10.1002/anie.201104765.

21. C. Zeng, W. Shang, X. Liang, et al., "Cancer Diagnosis and Imaging-Guided Photothermal Therapy Using a Dual-Modality Nanoparticle," *ACS Applied Materials & Interfaces* 8 (2016): 29232–29241, https://doi.org/10.1021/acsami.6b06883.

22. C. N. LaFratta, J. T. Fourkas, T. Baldacchini, and R. A. Farrer, "Multiphoton Fabrication," *Angewandte Chemie International Edition* 46 (2007): 6238–6258, https://doi.org/10.1002/anie.200603995.

23. M. Jin, J. Xie, J. P. Malval, et al., "Two-Photon Lithography in Visible and NIR Ranges Using Multibranched-Based Sensitizers for Efficient Acid Generation," *Journal of Materials Chemistry C* 2 (2014): 7201–7215, https://doi.org/10.1039/C4TC00706A.

24. W. Zhou, S. M. Kuebler, K. L. Braun, et al., "An Efficient Two-Photon-Generated Photoacid Applied to Positive-Tone 3D Microfabrication," *Science* 296 (2002): 1106–1109, https://doi.org/10.1126/science.296.5570.1106.

25. B. H. Cumpston, S. P. Ananthavel, S. Barlow, et al., "Two-Photon Polymerization Initiators for Three-Dimensional Optical Data Storage and Microfabrication," *Nature* 398 (1999): 51–54, https://doi.org/10.1038/17989.

26. S. Miao, Y. Zhu, H. Zhuang, et al., "Adjustment of Charge Trap Number and Depth in Molecular Backbone to Achieve Tunable Multilevel Data Storage Performance," *Journal of Materials Chemistry C* 1 (2013): 2320, https://doi.org/10.1039/c3tc00745f.

27. F. Hao, X. Zhang, Y. Tian, et al., "Design, Crystal Structures and Enhanced Frequency-upconverted Lasing Efficiencies of a New Series of Dyes From Hybrid of Inorganic Polymers and Organic Chromophores," *Journal of Materials Chemistry* 19 (2009): 9163, https://doi.org/10.1039/b914656c.

28. S. Casa and M. Henary, "Synthesis and Applications of Selected Fluorine-Containing Fluorophores," *Molecules (Basel, Switzerland)* 26 (2021): 1160, https://doi.org/10.3390/molecules26041160.

29. G. Chandra, B. Mahto, V. R. Singh, G. K. Mahato, and U. Rani, "Fluorescent Fluorinated Materials: A Novel Material for Application in Photodynamic Therapy and Designing Chemical Sensors," *Journal of Photochemistry and Photobiology C: Photochemistry Reviews* 60-61 (2024): 100677, https://doi.org/10.1016/j.jphotochemrev.2024.100677.

30. C. Martinelli, G. M. Farinola, V. Pinto, and A. Cardone, "Synthetic Aspects and Electro-Optical Properties of Fluorinated Arylenevinylenes

for Luminescence and Photovoltaics," *Materials* 6 (2013): 1205–1236, https://doi.org/10.3390/ma6041205.

31. R. Berger, G. Resnati, P. Metrangolo, E. Weber, and J. Hulliger, "Organic Fluorine Compounds: A Great Opportunity for Enhanced Materials Properties," *Chemical Society Reviews* 40 (2011): 3496, https://doi.org/10.1039/c0cs00221f.

32. C. Botta, E. Cariati, G. Cavallo, et al., "Fluorine-induced J-aggregation Enhances Emissive Properties of a New NLO Push–pull Chromophore," *Journal of Materials Chemistry C* 2 (2014): 5275, https://doi.org/10.1039/c4tc00665h.

33. N. Bauer, Q. Zhang, J. J. Rech, et al., "The Impact of Fluorination on both Donor Polymer and Non-Fullerene Acceptor: The More Fluorine, the Merrier," *Nano Research* 12 (2019): 2400–2405, https://doi.org/10.1007/s12274-019-2362-3.

34. J. M. W. Chan, "Pentafluorosulfanyl Group: An Emerging Tool in Optoelectronic Materials," *Journal of Materials Chemistry C* 7 (2019): 12822–12834, https://doi.org/10.1039/C9TC01949A.

35. G. J. Mohr, F. Lehmann, U.-W. Grummt, and U. E. Spichiger-Keller, "Fluorescent Ligands for Optical Sensing of Alcohols: Synthesis and Characterization of *p-N,N*-Dialkylamino-Trifluoroacetylstilbenes," *Analytica Chimica Acta* 344 (1997): 215, https://doi.org/10.1016/S0003-2670(97)00113-X.

36. Y. Xu, S. Yu, Y. Wang, et al., "Ratiometric Fluorescence Sensors for 1,2-Diamines Based on Trifluoromethyl Ketones," *European Journal of Organic Chemistry* 2016 (2016): 5868–5875, https://doi.org/10.1002/ejoc.201601157.

37. N. Aknine and A. S. Klymchenko, "Push–Pull Fluorescent Dyes With Trifluoroacetyl Acceptor for High-Fidelity Sensing of Polarity and Heterogeneity of Lipid Droplets," *Analytical Chemistry* 96 (2024): 13242–13251, https://doi.org/10.1021/acs.analchem.4c02322.

38. G. Landelle, A. Panossian, and F. Leroux, "Trifluoromethyl Ethers and –Thioethers as Tools for Medicinal Chemistry and Drug Discovery," *Current Topics in Medicinal Chemistry* 14 (2014): 941–951, https://doi.org/10.2174/1568026614666140202210016.

39. F. R. Leroux, B. Manteau, J. P. Vors, and S. Pazenok, "Trifluoromethyl Ethers—Synthesis and Properties of an Unusual Substituent," *Beilstein Journal of Organic Chemistry* 4, no. 13 (2008): 1–15, https://doi.org/10.3762/bjoc.4.13.

40. Z. Huang, S. Jia, C. Wang, E. Tokunaga, Y. Sumii, and N. Shibata, "New Utility of Electrophilic Trifluoromethylthiolation Reagents for the Synthesis of a Variety of Triflones," *Journal of Fluorine Chemistry* 198 (2017): 61–66, https://doi.org/10.1016/j.jfluchem.2016.12.012.

41. C. Hansch, A. Leo, and R. W. Taft, "A Survey of Hammett Substituent Constants and Resonance and Field Parameters," *Chemical Reviews* 91 (1991): 165–195, https://doi.org/10.1021/cr00002a004.

42. K. N. Lee, Z. Lei, C. A. Morales-Rivera, P. Liu, and M. Y. Ngai, "Mechanistic Studies on Intramolecular C-H Trifluoromethoxylation of (Hetero)Arenes via OCF_3-Migration" *Organic & Biomolecular Chemistry* 14 (2016): 5599, https://doi.org/10.1039/C6OB00132G.

43. Z. Li, Z. Wu, W. Fu, et al., "Versatile Fluorinated Derivatives of Triphenylamine as Hole-Transporters and Blue-Violet Emitters in Organic Light-Emitting Devices," *Journal of Physical Chemistry C* 116 (2012): 20504–20512, https://doi.org/10.1021/jp3028929.

44. E. Ripaud, C. Mallet, M. Allain, P. Leriche, P. Frre, and J. Roncali, "Extended Triphenylamine Conjugated Systems Derivatized by Perfluorophenyl Groups," *Tetrahedron Letters* 52 (2011): 6573–6577, https://doi.org/10.1016/j.tetlet.2011.09.129.

45. Y. Ban, L. Hao, Z. Peng, L. Sun, L. Teng, and Y. Zhao, "Triphenylamine-Based Highly Active Two-Photon Absorbing Chromophores With Push-Pull Systems," *Chinese Chemical Letters* 34 (2023): 107880, https://doi.org/10.1016/j.cclet.2022.107880.

46. S. P. McIlroy, E. Cló, L. Nikolajsen, et al., "Two-Photon Photosensitized Production of Singlet Oxygen: Sensitizers With Phenylene–Ethynylene-Based Chromophores," *Journal of Organic Chemistry* 70 (2005): 1134–1146, https://doi.org/10.1021/jo0482099.

47. E. Tatsi, V. Raglione, G. R. Ragno, et al., "Luminescent Solar Concentrators Based on Environmentally Friendly Tripodal D-(π-A)$_3$ Triarylamine Luminophores," *Journal of Materials Chemistry C* 13 (2025): 14465, https://doi.org/10.1039/D5TC01559F.

48. B. Kumari, S. P. Singh, R. Santosh, et al., "Branching Effect on Triphenylamine-CF_3 Cyanostilbenes: Enhanced Emission and Aggregation in Water," *New Journal of Chemistry* 43 (2019): 4106, https://doi.org/10.1039/C8NJ05907A.

49. P. Gautam, Y. Wang, G. Zhang, H. Sun, and J. M. W. Chan, "Using the Negative Hyperconjugation Effect of Pentafluorosulfanyl Acceptors to Enhance Two-Photon Absorption in Push–Pull Chromophores," *Chemistry of Materials* 30 (2018): 7055–7066, https://doi.org/10.1021/acs.chemmater.8b02723.

50. M. Fecková, M. Klikar, C. Vourdaki, et al., "Selective Employment of Electronic Effects of the Pentafluorosulfanyl Group Across Linear and Tripodal Push-Pull Chromophores With Two-Photon Absorption," *Advanced Materials* 6 (2025): 5713, https://doi.org/10.1039/D5MA00350D.

51. S. Körsten and G. J. Mohr, "Star-Shaped Tripodal Chemosensors for the Detection of Aliphatic Amines," *Chemistry: A European Journal* 17 (2011): 969, https://doi.org/10.1002/chem.201000787.

52. L. Porrès, O. Mongin, C. Katan, et al., "Enhanced Two-Photon Absorption with Novel Octupolar Propeller-Shaped Fluorophores Derived From Triphenylamine," *Organic Letters* 6 (2004): 47, https://doi.org/10.1021/ol036041s.

53. C. L. E. Droumaguet, O. Mongin, M. H. V. Werts, and M. Blanchard-Desce, "Towards "Smart" Multiphoton Fluorophores: Strongly Solvatochromic Probes for Two-photon Sensing of Micropolarity," *Chemical Communications* (2005): 2802, https://doi.org/10.1039/b502585k.

54. C. Rouxel, C. L. E. Droumaguet, Y. Macé, et al., "Octupolar Derivatives Functionalized With Superacceptor Peripheral Groups: Synthesis and Evaluation of the Electron-Withdrawing Ability of Potent Unusual Groups," *Chemistry—A European Journal* 18 (2012): 12487–12497, https://doi.org/10.1002/chem.201103460.

55. C. L. E. Droumaguet, A. Sourdon, E. Genin, O. Mongin, and M. Blanchard-Desce, "Two-Photon Polarity Probes Built From Octupolar Fluorophores: Synthesis, Structure-Properties Relationships, and Use in Cellular Imaging," *Chemistry - An Asian Journal* 8 (2013): 2984, https://doi.org/10.1002/asia.201300735.

56. M. Morita, S. Yamada, and T. Konno, "Systematic Studies on the Effect of Fluorine Atoms in Fluorinated Tolanes on Their Photophysical Properties," *Molecules (Basel, Switzerland)* 26 (2021): 2274, https://doi.org/10.3390/molecules26082274.

57. K. E. Johannessen, M. A. L. Johansen, R. F. Einrem, et al., "Influence of Fluorinated Substituents on the Near-Infrared Phosphorescence of 5d Metallocorroles," *ACS Organic & Inorganic Au* 3 (2023): 241–245, https://doi.org/10.1021/acsorginorgau.3c00016.

58. D. Chen and E. Zysman-Colman, "Exploring the Possibility of Using Fluorine-Involved Non-Conjugated Electron-Withdrawing Groups for Thermally Activated Delayed Fluorescence Emitters by TD-DFT Calculation," *Beilstein Journal of Organic Chemistry* 17 (2021): 210–223, https://doi.org/10.3762/bjoc.17.21.

59. M. Klikar, D. Georgiou, I. Polyzos, et al., "Triphenylamine-Based Fluorophores Bearing Peripheral Diazine Regioisomers. Synthesis, Characterization, Photophysics and Two-Photon Absorption," *Dyes and Pigments* 201 (2022): 110230, https://doi.org/10.1016/j.dyepig.2022.110230.

60. M. Klikar, K. Seintis, I. Polyzos, et al., "Star-Shaped Push-Pull Molecules With a Varied Number of Peripheral Acceptors: An Insight Into Their Optoelectronic Features," *ChemPhotoChem* 2 (2018): 465–474, https://doi.org/10.1002/cptc.201800051.

61. D. Cvejn, E. Michail, I. Polyzos, et al., "Modulation of (Non)Linear Optical Properties in Tripodal Molecules by Variation of the Peripheral

Cyano Acceptor Moieties and the π-Spacer," *Journal of Materials Chemistry C* 3 (2015): 7345–7355, https://doi.org/10.1039/C5TC01293G.

62. J. Kulhánek, Z. Burešová, M. Klikar, et al., "Synthesis, Photophysics and Two-Photon Absorption of Imidazole-Centred Tripodal Chromophores," *Physical Chemistry Chemical Physics* 26 (2024): 20908–20918, https://doi.org/10.1039/D4CP02227K.

63. D. Cvejn, E. Michail, K. Seintis, et al., "Solvent and Branching Effect on the Two-Photon Absorption Properties of Push-Pull Triphenylamine Derivatives," *RSC Advances* 6 (2016): 12819, https://doi.org/10.1039/C5RA25170B.

64. B. L. Edelbach, B. M. Pharoah, S. M. Bellows, et al., "An Expedient Synthesis of 2,4,6-Tris(trifluoromethyl)aniline," *Synthesis* 44 (2012): 3595, https://doi.org/10.1055/s-0032-1316809.

65. S. Mori, N. Tsuemoto, T. Kasagawa, E. Nakano, S. Fujii, and H. Kagechika, "Development of Boron-Cluster-Based Progesterone Receptor Antagonists Bearing a Pentafluorosulfanyl (SF₅) Group," *Chemical and Pharmaceutical Bulletin* 67 (2019): 1278–1283, https://doi.org/10.1248/cpb.c19-00522.

66. Z. Liu, W. Wei, L. Xiong, et al., "Selective and Efficient Synthesis of Trans-arylvinylboronates and Trans-hetarylvinylboronates Using Palladium Catalyzed Cross-Coupling," *New Journal of Chemistry* 41 (2017): 3172–3176, https://doi.org/10.1039/C6NJ03984G.

67. T. J. Carter, R. Mohtadi, T. S. Arthur, et al., "Boron Clusters as Highly Stable Magnesium-Battery Electrolytes," *Angewandte Chemie International Edition* 53 (2014): 3173–3177, https://doi.org/10.1002/anie.201310317.

68. A. A. Isse and A. Gennaro, "Absolute Potential of the Standard Hydrogen Electrode and the Problem of Interconversion of Potentials in Different Solvents," *Journal of Physical Chemistry B* 114 (2010): 7894–7899, https://doi.org/10.1021/jp100402x.

69. D. T. Sawyer, A. Sobkowiak, and J. L. Roberts Jr, *Electrochemistry for Chemists*. 2nd edition (New York, Chichester: Wiley-Interscience, 1995): 1–528.

70. O. Exner and S. Böhm, "Negative Hyperconjugation of some Fluorine Containing Groups," *New Journal of Chemistry* 32 (2008): 1449, https://doi.org/10.1039/b718430a.

71. F. Bureš, O. Pytela, and F. Diederich, "Solvent Effects on Electronic Absorption Spectra of Donor-Substituted 11,11,12,12-Tetracyano-9,10-anthraquinodimethanes (TCAQs)," *Journal of Physical Organic Chemistry* 22 (2009): 155, https://doi.org/10.1002/poc.1443.

72. A. M. Brouwer, "Standards for Photoluminescence Quantum Yield Measurements in Solution (IUPAC Technical Report)," *Pure and Applied Chemistry* 83 (2011): 2213–2228, https://doi.org/10.1351/PAC-REP-10-09-31.

73. M. Klikar, I. V. Kityk, D. Kulwas, T. Mikysek, O. Pytela, and F. Bureš, "Multipodal Arrangement of Push–pull Chromophores: A Fundamental Parameter Affecting Their Electronic and Optical Properties," *New Journal of Chemistry* 41 (2017): 1459–1472, https://doi.org/10.1039/C6NJ02994A.

74. S. K. Suresh, L. M. Ramachandran, A. Krishnan, and C. V. Suneesh, "The Effect of –CF3 Substitution Position on the Aggregation-induced Emission, Solvatofluorochromism and Mechanofluorochromism Properties of the Conjugated 9-butyl-9H-carbazole Phenylacrylonitrile Derivatives," *Journal of Photochemistry and Photobiology A: Chemistry* 444 (2023): 114985, https://doi.org/10.1016/j.jphotochem.2023.114985.

75. F. Bureš, "Fundamental Aspects of Property Tuning in Push-Pull Molecules," *RSC Advances* 4 (2014): 58826, https://doi.org/10.1039/C4RA11264D.

76. P. Swiderek, M. Michaud, and L. Sanche, "Vibronic Structure in the Low-lying Singlet–triplet Transitions of Benzene and Toluene," *Journal of Chemical Physics* 105 (1996): 6724–6732, https://doi.org/10.1063/1.471852.

77. A. R. Nair, M. G. Mohan, C. Raksha, et al., "Unveiling the Dual-State Emissive Behaviour of 4,6-Diarylpyrimidin-2-amines Through a Plug-and-play Approach," *Scientific Reports* 14 (2024): 29795, https://doi.org/10.1038/s41598-024-81723-1.

78. Z. Shi, J. Davies, S. H. Jang, W. Kaminsky, and A. K. Y. Jen, "Aggregation Induced Emission (AIE) of Trifluoromethyl Substituted Distyrylbenzenes," *Chemical Communications* 48 (2012): 7880, https://doi.org/10.1039/C2CC32380J.

79. M. J. Frisch, G. W. Trucks, H. B. Schlegel, et al., Gaussian®16 W Software Package, Program for the Theoretical (TD-)DFT Calculations, Wallingford (USA), 2016.

80. D. M. Chang, D. Y. Kwon, and Y. S. Kim, "Heteroleptic Dual Acceptor Organic Dyes With Rhodanine-3-acetic Acid and Cyanoacrylic Acid," *Molecular Crystals and Liquid Crystals* 585 (2013): 100–106, https://doi.org/10.1080/15421406.2013.850933.

81. M. Fakis, V. Petropoulos, P. Hrobárik, et al., "Exploring Solvent and Substituent Effects on the Excited State Dynamics and Symmetry Breaking of Quadrupolar Triarylamine End-Capped Benzothiazole Chromophores by Femtosecond Spectroscopy," *Journal of Physical Chemistry B* 126 (2022): 8532–8543, https://doi.org/10.1021/acs.jpcb.2c03103.

82. K. Seintis, Ç. Şahin, I. Sigmundová, E. Stathatos, P. Hrobárik, and M. Fakis, "Solvent-Acidity-Driven Change in Photophysics and Significant Efficiency Improvement in Dye-Sensitized Solar Cells of a Benzothiazole-Derived Organic Sensitizer," *Journal of Physical Chemistry C* 122 (2018): 20122–20134, https://doi.org/10.1021/acs.jpcc.8b05686.

83. C. Xu and W. W. Webb, "Measurement of Two-Photon Excitation Cross Sections of Molecular Fluorophores With Data From 690 to 1050 Nm," *Journal of the Optical Society of America B* 13 (1996): 481, https://doi.org/10.1364/JOSAB.13.000481.

84. N. S. Makarov, M. Drobizhev, and A. Rebane, "Two-Photon Absorption Standards in the 550–1600 Nm Excitation Wavelength Range," *Optics Express* 16 (2008): 4029, https://doi.org/10.1364/OE.16.004029.

85. X. Zeng, C. Gong, H. Guo, H. Xu, J. Zhang, and J. Xie, "Efficient Heterogeneous Hydroboration of Alkynes: Enhancing the Catalytic Activity by Cu(0) Incorporated $CuFe_2O_4$ Nanoparticles," *New Journal of Chemistry* 42 (2018): 17346, https://doi.org/10.1039/C8NJ03708F.

86. A. Payet, B. Blondeau, J. B. Behr, and J. L. Vasse, "Synthesis of 1,3-disubstituted Cyclohexenes From Dienylethers via Sequential Hydrozirconation/Deoxygenative Cyclisation," *Organic & Biomolecular Chemistry* 17 (2019): 798–802, https://doi.org/10.1039/C8OB02925C.

87. M. Wu, C. Yan, D. Zhuang, and R. Yan, "Metal-Free C–S Bond Formation in Elemental Sulfur and Cyclobutanol Derivatives: The Synthesis of Substituted Thiophenes," *Organic Letters* 24 (2022): 5309–5313, https://doi.org/10.1021/acs.orglett.2c01907.

88. K. Itami, T. Nokami, Y. Ishimura, K. Mitsudo, T. Kamei, and J.-I. Yoshida, "Diversity-Oriented Synthesis of Multisubstituted Olefins Through the Sequential Integration of Palladium-Catalyzed Cross-Coupling Reactions. 2-Pyridyldimethyl(vinyl)Silane as a Versatile Platform for Olefin Synthesis," *Journal of the American Chemical Society* 123 (2001): 11577–11585, https://doi.org/10.1021/ja016790+.

89. M. H. Aukland, F. J. T. Talbot, J. A. Fernández-Salas, M. Ball, A. P. Pulis, and D. J. Procter, "An Interrupted Pummerer/Nickel-Catalysed Cross-Coupling Sequence," *Angewandte Chemie International Edition* 57 (2018): 9785–9789, https://doi.org/10.1002/anie.201805396.

90. J. Qu, C. T. Cao, and C. Cao, "Determining the Excited-state Substituent Constants of Furyl and Thienyl Groups," *Journal of Physical Organic Chemistry* 31 (2018): e3799, https://doi.org/10.1002/poc.3799.

91. A. Vasseur, J. Muzart, and J. L. E. Bras, "Dehydrogenative Heck Reaction of Furans and Thiophenes With Styrenes Under Mild Conditions and Influence of the Oxidizing Agent on the Reaction Rate," *Chemistry—A European Journal* 17 (2011): 12556–12560, https://doi.org/10.1002/chem.201101992.

92. L. U. Colmenares and R. S. H. Liu, "Fluorine-19 NMR Evidence for Restricted Rotation of the Retinyl Chromophore in Doubly Labeled Visual Pigment Analogs," *Journal of the American Chemical Society* 114 (1992): 6933–6934, https://doi.org/10.1021/ja00043a058.

93. R. Chen, L. U. Colmenares, J. R. Thiel, and R. S. I. Liu, "Spiral Hexatrienes. The Hindered Cis Isomer of Mini-carotene-3 and Hexakis-(2,2',4,4',6,6'-trifluoromethyl)stilbene," *Tetrahedron Letters* 35 (1994): 7177, https://doi.org/10.1016/0040-4039(94)85354-1.

94. L. U. Colmenares and R. S. H. Liu, "Fluorinated Phenylrhodopsin Analogs. Binding Selectivity, Restricted Rotation and 19F-NMR Studies. Binding Selectivity, Restricted Rotation and ^{19}FNMR Studies," *Tetrahedron* 52 (1996): 109–118, https://doi.org/10.1016/0040-4020(95)00887-E.

95. G. M. Sheldrick, SHELXL-97, Program for Crystal Structure Refinement, Göttingen (Germany) (2008). University of Göttingen.

96. O. Pytela, OPChem, (n.d.)., Program for Visualization of Structures Pardubice (Czechia) (2023). University of Pardubice.

97. O. Pytela, OPStat, (n.d.)., Program for Mathematical and Statistical Calculations Pardubice (Czechia) (2018). University of Pardubice.

Supporting Information

Additional supporting information can be found online in the Supporting Information section.

The authors have cited additional references within the Supporting Information [81–97]. The data supporting this article have been included as part of the SI, and the dataset available at https://doi.org/10.6084/m9.figshare.30646283. Crystallographic data for **2aL** has been deposited at the [CCDC] under [2502796] and can be obtained from [https://www.ccdc.cam.ac.uk]. **Supporting File 1**: chem70633-sup-0001-SuppMat.pdf. **Supporting File 2**: chem70633-sup-0002-Data.zip.